Macrophage-secreted granulin supports pancreatic cancer metastasis by inducing liver fibrosis

Published in final edited form as:
Nat Cell Biol. 2016 May ; 18(5): 549–560. doi:10.1038/ncb3340.

Macrophage-secreted granulin supports pancreatic cancer metastasis by inducing liver fibrosis

Sebastian R Nielsen[1], **Valeria Quaranta**[1], **Andrea Linford**[1], **Perpetua Emeagi**[1], **Carolyn Rainer**[1], **Almudena Santos**[1], **Lucy Ireland**[1], **Takao Sakai**[2], **Keiko Sakai**[2], **Yong-Sam Kim**[3,4], **Dannielle Engle**[5,6], **Fiona Campbell**[1], **Daniel Palmer**[1], **Jeong Heon Ko**[3,4], **David A. Tuveson**[5,6,7], **Emilio Hirsch**[8], **Ainhoa Mielgo**[1], and **Michael C Schmid**[1,*]

[1]Department of Molecular and Clinical Cancer Medicine, University of Liverpool, Daulby Street, Liverpool, L69 3GA, UK

[2]Department of Molecular and Clinical Pharmacology, University of Liverpool, Ashton Street, Liverpool, L69 3GE, UK

[3]Aging Intervention Research Center, KRIBB, 125 Gwahak-ro, Yuseong-gu, Deajeon 305-806, Korea

[4]Korea University of Science and Technology, 217 Gajeong-ro, Yuseong-gu, Daejeon 305-350, Korea

[5]Cold Spring Harbor Laboratory, Cold Spring Harbor, NY 11724, USA

[6]Lustgarten Pancreatic Cancer Research Laboratory, Cold Spring Harbor, NY 11724, USA

[7]Rubenstein Center for Pancreatic Cancer Research, Memorial Sloan Kettering Cancer Center, New York, NY 10065, USA

[8]Department of Molecular Biotechnology and Health Sciences, Center for Molecular Biotechnology, University of Torino, Via Nizza 52, 10126 Turin, Italy

Abstract

Pancreatic ductal adenocarcinoma (PDAC) is a devastating metastatic disease for which better therapies are urgently needed. Macrophages enhance metastasis in many cancer types, however, the role of macrophages in PDAC liver metastasis remains poorly understood. Here we found that PDAC liver metastasis critically depends on the early recruitment of granulin secreting inflammatory monocytes to the liver. Mechanistically, we demonstrate that granulin secretion by

*to whom correspondence should be addressed mschmid@liv.ac.uk.

Author contributions

S.R.N. designed and performed most of the experiments, analysed and interpreted the data, and contributed to the preparation of the manuscript. V.Q. performed qPCR experiments, immunofluorescence stainings, and immunoblotting. A.L. performed human immune cell analysis and immunohistochemistry. V.Q., P.E., A.S. L.I. helped with *in vivo* experiments. C.R performed flow cytometry and cell sorting. A.S. performed immunohistochemistry. K.T. and S.T. provided primary and immortalised hStCs. Y.S.K. and J.H.K. performed proteomic analysis. D.E. and D.T. provided primary murine KPC-derived pancreatic cancer cells. F.C helped with the analysis and interpretation of tumour biopsies. D.P. provided patient samples. E.H. provided PI3K$\gamma^{-/-}$ mouse colony. A.M. provided conceptual advice, designed experiments, and wrote the manuscript. M.C.S. conceived and supervised the project, interpreted data, and wrote the manuscript. All authors critically analysed and approved the manuscript.

Europe PMC Funders Author Manuscripts

metastasis associated macrophages (MAMs) activates resident hepatic stellate cells (hStCs) into myofibroblasts that secrete periostin, resulting in a fibrotic microenvironment that sustains metastatic tumour growth. Disruption of MAM recruitment or genetic depletion of granulin reduced hStCs activation and liver metastasis. Interestingly, we found that circulating monocytes and hepatic MAMs in PDAC patients express high levels of granulin. These findings suggest that recruitment of granulin expressing inflammatory monocytes plays a key role in PDAC metastasis and may serve as a potential therapeutic target for PDAC liver metastasis.

Introduction

Pancreatic cancer is among the most lethal cancers in part due to its aggressive metastatic nature 1, 2. Metastatic spreading is a multistage process, which starts with the dissemination of cancer cells from the primary tumour site and ends with clinically detectable metastatic outgrowth at distant organs. Tumours can release large numbers of cancer cells into the circulation, but only a small proportion of these cells are able to successfully survive and colonise the hostile environment at the distant metastatic site 3, 4. Thus, the successful outgrowth of metastatic tumour cells in this new distant environment is a severe rate limiting step during metastasis. Emerging evidence indicates that the colonisation of a new organ by metastatic tumour cells critically depends on the support of non-cancerous stromal partners 5–8. Multiple steps of the metastatic cascade are supported by stromal partners, particularly macrophages and, in many cancers, metastasis correlates with increased macrophages at the metastatic site 9–14. PDAC is characterised by its formation of ductal structures and a rich stromal compartment containing mainly fibroblasts, stellate cells and infiltrating immune cells. In response to the presence of tumour cells, quiescent fibroblasts and stellate cells become activated myofibroblasts that express alpha smooth muscle actin (αSMA) 15. In non-pathological conditions, myofibroblasts are critical for wound healing 16. In cancer, the role of myofibroblasts is currently controversial. Previous studies have suggested that myofibroblasts support tumour growth and restrict the delivery of chemotherapeutic drugs to the tumour 17–19. However, recent reports have shown that genetic depletion of myofibroblasts results in tumour progression and metastasis 20, 21. Most pancreatic cancer studies have focused on the role of stromal partners at the primary site, however, the role of stromal cells at the secondary metastatic site, which for PDAC is most often the liver, remains poorly understood.

At the moment, the best treatment option for PDAC patients is resection of the pancreatic tumour, but, unfortunately, by the time PDAC patients are diagnosed, the majority (~ 80%) present with non-resectable metastatic cancer. Moreover, more than 60% of the patients whose tumours are resected, relapse with distant hepatic recurrence within the first 24 months after surgery 22, 23. Thus, a better understanding of the mechanisms underlying the metastatic process in pancreatic cancer is critical to improve treatment and patient outcome.

Europe PMC Funders Author Manuscripts

Results

Metastatic PDAC cells trigger macrophage recruitment and an extensive stromal response in the liver

The most common route of PDAC metastasis is to the liver. To understand whether and how stromal cells influence liver PDAC metastasis, we first analysed liver biopsies from advanced metastatic PDAC patients and healthy volunteers by immunohistochemical (IHC) and immunofluorescence (IF) techniques. We found that metastatic tumour cells (cytokeratin$^+$) are surrounded by an abnormal stromal compartment rich in hematopoietic immune cells (CD45$^+$), macrophages (CD68$^+$), myofibroblasts (αSMA$^+$; PDGFRα^+) and connective tissue deposition (Fig. 1a and Supplementary Fig. 1a-c). To further evaluate the type of immune cells accumulating at the metastatic site, we intrasplenically injected KPC-derived cells (FC1199), isolated from the genetically engineered mouse model of PDAC (Kras^{G12D};Trp53^{R172H};Pdx1-Cre mice) 24. In this model, tumour cells migrate to the liver via the portal circulation (a common way of metastasis occurring in humans) 25, 26, and generate metastases restricted to the liver (Supplementary Fig. 1d). We analysed established metastatic tumours at day 12, by flow cytometry, and found that the percentage of CD45$^+$ immune cells, B220$^+$ B cells, CD3$^+$ T cells, Nk1.1$^+$ NK cells, CD11b$^+$Ly6G$^+$ neutrophils, and F4/80$^+$ macrophages were increased in tumour bearing livers compared to tumour free livers (Supplementary Fig. 2a-c). However, among the CD45$^+$ immune cells, metastasis associated macrophages (MAM; CD11b$^+$F4/80$^+$Ly6G^{neg}CCR2$^+$) were the most predominant cell population (Fig. 1b, Supplementary Fig. 2d and Supplementary Fig. 3a, b). Interestingly, metastatic tumour cells initially induced a rapid accumulation of CD11b$^+$F4/80^{neg}Ly6C$^+$LY6G^{neg}CCR2$^+$ inflammatory monocytes (IM) followed by an accumulation of MAMs (Supplementary Fig. 3a). In contrast, accumulation of αSMA$^+$ myofibroblasts and stromal expansion, were detected only in established experimental and spontaneous metastatic lesions (Fig. 1c, d and Supplementary Fig. 3b - g)

Macrophages in the liver can be broadly categorised into two classes: embryonically derived tissue-resident macrophages known as Kupffer cells (KC), and infiltrating macrophages derived from IM that originate from the bone marrow 27–30. To investigate whether the increased MAMs we observe is due to an expansion of resident KC or to the recruitment of BM-derived cells, we generated bone marrow chimeras by engrafting tdTomato red (tdTomato) BM into irradiated wild type mice (WT + tdTomato$^+$ BM) or WT BM into irradiated WT mice (WT + WT BM). Since KCs in the liver are radio-resistant 31, they remain of host origin and are therefore F4/80$^+$ tdTomato^{neg}, whereas BM-derived macrophages are of donor origin and F4/80$^+$ tdTomato$^+$ (Fig. 1e). After confirming successful BM reconstitution (Supplementary Fig. 3h), chimeric mice were intrasplenically implanted with the murine PDAC cell line Panc02 32. We found that MAMs were exclusively tdTomato$^+$, and thus, derived from BM (Fig. 1f and Supplementary Fig. 3i). Conversely, in adjacent “normal liver tissue”, F4/80$^+$ macrophages, remained tdTomato^{neg}, consistent with resident F4/80$^+$ KC (Fig. 1f). In addition, αSMA$^+$ metastasis associated myofibroblasts remained tdTomato^{neg}, suggesting that these cells are not from BM origin, but are locally activated mesenchymal cells, such as resident hepatic stellate cells (hStCs) or fibroblasts (Fig. 1f and Supplementary Fig. 3j). Together, our findings demonstrate that i) in

PDAC liver metastasis, MAMs originate from IM, ii) MAMs represent the predominant immune cell population in metastatic liver lesions, and iii) MAM accumulation in the liver precedes myofibroblast activation.

Macrophages promote myofibroblast activation and metastatic growth

To determine the functional role of MAMs in pancreatic cancer metastasis, we next intrasplenically implanted KPC cells into isogenic PI3K$\gamma^{-/-}$ mice (p110$\gamma^{-/-}$) 33 and control WT mice. PI3K$\gamma$is mainly expressed in the hematopoietic compartment, and PI3Kγ knockout mice have a defect in monocyte recruitment in response to inflammatory and tumour derived signals 34, 35. Since we previously found that MAMs are IM-derived macrophages that are actively recruited from the BM to the metastatic liver (Fig. 1f), we hypothesised that depletion of PI3Kγ will ablate IM trafficking to the metastatic site and consequently abolish MAM accumulation in the liver. Indeed, macrophage and IM numbers were significantly reduced in metastatic livers of PI3K$\gamma^{-/-}$ mice compared to WT mice as measured by flow cytometry analysis (Fig. 2a). Importantly, PI3Kγ depletion markedly reduced metastatic frequency, average metastatic lesion size, and αSMA^{+} myofibroblast numbers, in both KPC (Fig. 2b - d and Supplementary Fig. 4a) and Panc02 (Supplementary Fig. 4b - e) liver metastasis bearing mice. Together, these results suggest that inhibition of BM-derived macrophage recruitment to the liver prevents pancreatic cancer metastasis to the liver and is accompanied by a decrease in myofibroblast activation.

Since the majority (~ 80%) of PDAC patients, present with liver metastases at time of diagnosis, or relapse with hepatic recurrence after surgical removal of primary pancreatic tumours 1, we next focused our studies on investigating whether MAMs are required for supporting the metastatic growth of already disseminated cancer cells. To address this question, we chemically depleted MAMs *in vivo*, using clodronate liposomes (CL)36. CL treatment was started at day 3 post intrasplenic injection of KPC cells, a time point in which initial seeding of the liver by KPC cells has already occurred (Fig. 2e and Supplement Fig. 5a, b). As expected, in response to CL treatment, MAM numbers were significantly reduced (Fig. 2f and Supplementary Fig. 5c). Interestingly, we could barely detect any αSMA^{+} myofibroblasts in metastatic livers of CL treated mice (Fig. 2f and Supplementary Fig. 5c). The ablation of MAMs and the prevention of αSMA^{+} myofibroblast accumulation was not cell line specific since similar results were observed using Panc02 cells (Supplementary Fig. 5d, e). Although the metastatic frequency was only modestly affected by CL treatment in both models, the size of the lesion area covered by metastatic cells was significantly reduced in response to macrophage depletion (Fig. 2g, h and Supplementary Fig. 5f, g). Together, these results suggest that depletion of MAMs prevents the activation of myofibroblasts and impairs the progression of metastatic lesions even after initial colonisation of the metastatic site by cancer cells.

Granulin secreted by macrophages triggers myofibroblast activation

We next sought to understand how MAMs regulate myofibroblast activation at the metastatic site. In this respect, we found that macrophage conditioned media (CM) acts as a strong activator of quiescent primary fibroblasts in culture and enhances their invasion and proliferation (Supplementary Fig. 6a-c). To identify the macrophage-derived factors

responsible for myofibroblast activation, we next exposed human THP-1 macrophages to the pancreatic cancer cell line Panc1 CM *in vitro*, and performed a secretome analysis. We identified several extracellular matrix proteases associated with macrophage function 37–39 (Supplementary Table 1, 2). Among the most highly secreted proteins we identified granulin (Grn), an approximately 70 kDa secreted glycoprotein that has previously been shown to mediate wound healing, by stimulating fibroblast migration 40, and to induce fibrosis in breast cancer 41. Since the main source of myofibroblasts in the liver are activated resident hStCs (Supplementary Fig. 3j) 16, we next isolated primary hStCs from mice and stimulated them with CM generated from primary murine WT BM derived macrophages or $Grn^{-/-}$ (granulin deficient) murine BM macrophages (BMM). We found that CM generated from WT, but not from $Grn^{-/-}$, BMM efficiently activated isogenic hStCs and promoted their migration (Fig. 3a, b). Importantly, addition of recombinant granulin to $Grn^{-/-}$ BMM CM was sufficient to restore hStCs activation and migration (Fig. 3a, b). Next, we isolated MAMs from tumour bearing livers derived from chimeric WT + WT BM and WT + $Grn^{-/-}$ BM mice, and prepared MAM CM. We confirmed that only CM from WT MAMs efficiently induced hStCs activation and migration, while CM from $Grn^{-/-}$ MAM was unable to induce activation or migration of hStCs (Fig. 3c - e). In addition, we found that granulin expression and secretion is increased in tumour educated (Fig. 3f, g) and alternatively (M2-like) activated macrophages (Supplementary Fig. 6d, e). Together, these data indicate that cancer cell derived factors induce the secretion of granulin in macrophages and that MAMs activate resident hStCs via granulin.

Granulin is highly expressed in pancreatic cancer metastatic lesions of mice and humans and MAMs are the main source of granulin in vivo

In vivo, we found that within the metastatic tumour microenvironment, granulin is highly expressed in MAMs, and that MAMs are the main source of granulin secretion in metastatic lesions (Fig. 4a, b). When we analysed chimeric mice harbouring tdTomatoRed BM, we found that BM derived MAMs, but not resident KC, express high levels of *granulin* (Fig. 4c). Surprisingly, expression levels of *Tgfb*, a common activator of hStCs 42, were low in MAMs and KC (Fig. 4c).

Finally, we further confirmed that granulin is highly expressed in the stroma of spontaneous hepatic metastatic lesions of human and murine tissues 24 43 (Fig. 4d, e and Supplementary Fig. 6f). Taken together, our findings indicate that granulin is highly expressed by MAMs and that MAMs are the main source of granulin in PDAC liver metastasis.

Depletion of granulin prevents liver fibrosis and PDAC metastatic growth

To investigate whether granulin is required for PDAC metastatic progression *in vivo*, we next inoculated $Grn^{-/-}$ and WT mice with isogenic KPC cells through intrasplenic implantation. We observed that lack of granulin expression did not alter metastatic frequency since WT and $Grn^{-/-}$ mice showed similar numbers of metastatic nodules (Fig. 5a, b). However, the area covered by metastatic tumour cells in $Grn^{-/-}$ mice was significantly smaller compared to WT, resulting in an overall significant decrease of hepatic metastatic tumour burden (Fig. 5a, c). While depletion of granulin did not reduce the number of total MAMs (Fig. 5d), nor their polarisation at the metastatic site (Supplementary Fig. 7a),

granulin deficiency abolished the accumulation of activated myofibroblasts in metastatic liver lesions (Fig. 5d). Quantitative gene expression analysis of myofibroblast activation markers (*Acta2, Fn, Col1a1*) 16, further confirmed that lack of granulin prevents the activation of intrametastatic hStCs into myofibroblasts *in vivo* (Fig. 5e).

Next, we characterised metastatic pancreatic tumour growth in WT mice transplanted with BM from $Grn^{-/-}$ or WT animals. We found that depletion of granulin in the hematopoietic compartment was sufficient to suppress metastatic growth of KPC cells (Fig. 5f, g) and to prevent myofibroblast activation *in vivo* (Fig. 5h, i), while MAM numbers and polarisation remained unchanged (Fig. 5j and Supplementary Fig. 7b). Interestingly, ablation of granulin in the hematopoietic compartment markedly reduced the number of proliferating ($Ki67^{+}$) metastatic pancreatic tumour cells (Fig. 5k), while apoptotic (cleaved caspase 3^{+}) tumour cell numbers remained unchanged (Fig. 5l). Taken together, these results suggest that granulin secretion by MAMs is required for hStCs activation and for metastatic growth of pancreatic tumours in the liver.

Granulin induces periostin expression in hStCs thereby allowing tumour growth

Next, we sought to gain a better understanding of how MAM-induced myofibroblast activation promotes pancreatic cancer cell growth. To address this question, we stimulated human fibroblasts with macrophage CM and performed a mass spectrometry quantitative analysis of the secretome from fibroblasts exposed to macrophage CM compared to unexposed fibroblasts. We found that macrophage CM induces fibroblast secretion of proteins associated with ECM remodelling (Fig. 6a and Supplementary Table 3), and in particular the secretion of the ECM component periostin (Fig. 6b). Periostin has been reported to enhance metastatic growth of breast and colon cancer cells through activation of Wnt and $\alpha_V\beta3$-Akt/PKB signalling pathways, respectively 8, 44. Thus, we next tested whether periostin expression by activated myofibroblasts is necessary to promote pancreatic cancer cell survival and growth. We found that myofibroblasts CM markedly promoted colony formation and proliferation of PDAC cancer cells, and that addition of a periostin neutralising antibody completely abolished these effects (Fig. 6c, Supplementary Fig. 7c). We confirmed that periostin acts in a paracrine myofibroblast-tumour cell loop since we did not detect any periostin expression in PDAC cells (Supplementary Fig. 7d). Moreover, we found that periostin was markedly upregulated in spontaneous hepatic metastatic lesions of human and murine tissues compared to healthy control livers (Fig. 6d and Supplementary Fig. 7e). Importantly, the induction of periostin expression in primary hStCs was strictly dependent on granulin, since CM generated from $Grn^{-/-}$ BMM (Fig. 7a) and MAMs (Fig. 7b, c) was unable to induce periostin expression in hStCs. To examine whether inhibition of myofibroblasts activation by MAMs-derived granulin also affects periostin expression and stroma expansion *in vivo*, we analysed metastatic liver tissue sections of WT, $PI3K\gamma^{-/-}$, $Grn^{-/-}$, WT + $Grn^{-/-}$ BM, and WT+CL treated mice. In all models, hepatic periostin expression levels and connective tissue deposition were found to be significantly reduced compared to metastasis bearing WT control animals (Fig. 7d, e and Supplementary Fig. 7f, g). In agreement with these findings, we found that intrametastatic myofibroblasts isolated from $Grn^{-/-}$ and WT + $Grn^{-/-}$ BM mice showed an approximately threefold reduction in periostin expression relative to control myofibroblasts isolated from WT tumour lesions

(Fig. 7f). Taken together, these findings indicate that MAMs induce the expression of ECM proteins in myofibroblasts, particularly periostin, in a granulin-dependent manner which then supports metastatic pancreatic tumour growth.

Although less frequently, PDAC can also sometimes metastasise to the lung 1. Similar to what we observed in the liver, granulin was markedly expressed in the stromal compartment of pulmonary metastatic lesions, especially in areas rich in $CD68^{+}$ macrophages (Supplementary Fig. 8a). Depletion of granulin in the hematopoietic compartment (WT + $Grn^{-/-}$ BM) was sufficient to reduce pulmonary metastatic growth of PDAC cells, and to prevent myofibroblast activation, fibrotic stromal expansion, and periostin deposition *in vivo*, while MAM numbers remained unchanged (Supplementary Fig. 8b-e). To further explore whether this mechanism is specific for the metastatic site, we next analysed primary PDAC tumours for granulin and periostin expression. Interestingly, we found that at the primary tumour site granulin is mainly expressed by tumour cells, and not by macrophages, while periostin was strongly expressed in the surrounding stromal compartment (Supplement Fig. 8f).

Taken together, these data suggest that granulin expressing macrophages play a critical role at the metastatic site, but not at the primary tumour site.

Circulating IM from metastatic PDAC patients express granulin

Since granulin expressing MAMs originate from the BM, we next investigated whether circulating IM express granulin. Therefore, we collected fresh blood samples from PDAC patients with metastases, but prior to therapeutic intervention, and from healthy control subjects, and purified IM ($CD14^{hi}CD16^{neg}$) and resident monocytes (RM) ($CD14^{dim}CD16^{hi}$) by fluorescence-activating cell sorting 45. We found that the percentage of IMs isolated from metastatic PDAC patients was significantly higher compared with healthy subjects, while no differences were observed in the percentage of resident monocytes (Fig. 8a,b and Supplementary Fig. 8g). Importantly, IM isolated from PDAC patients and from metastatic KPC mice exhibited abnormally elevated *granulin* expression levels compared to healthy control subjects (Fig. 8c, d).

Discussion

In this study, we aimed to gain a better understanding of the role of macrophages in pancreatic cancer metastasis, with the hope to improve therapies for this devastating disease. In this respect, we found that MAMs support pancreatic cancer metastasis by secreting granulin, which consequently promotes the activation of resident hStCs into αSMA+ myofibroblasts that secrete high levels of periostin (Fig. 8e). Collectively, our studies provide a comprehensive functional analysis of stroma - tumour interaction in PDAC metastasis, and support the rationale for the development of therapeutic approaches targeting stromal secreted pro-metastatic factors such as granulin and periostin to disrupt the inter-relationship between MAMs, myofibroblasts and cancer cells. In addition, we observed an increase of granulin expressing IM in blood from metastatic PDAC patients and metastatic KPC mice compared to healthy subjects. This observation suggests that granulin could also potentially be used as a predictive biomarker of PDAC metastasis. However, to assess the

potential use of granulin as a predictive biomarker of PDAC metastasis, granulin expression levels in IM derived from inflammatory, non-cancerous diseases, such as pancreatitis, would be worth exploring in future analysis.

The fact that MAMs isolated from metastatic lesions secrete high levels of granulin, but resident macrophages (KC) do not (Fig. 4c), indicates that the recruitment of monocyte-derived macrophages is a critical step during PDAC metastasis. We and others have previously shown that cancer cells release chemotactic factors, including CCL2, SDF-1α and mCSF1, to attract pro-tumorigenic monocytes to the tumour, in a PI3Kγ-dependent manner 11, 35, 46–48. Consistent with this, we found that prevention of macrophage recruitment, resulted in decreased hStCs activation, reduced periostin levels and decreased metastasis to the liver.

Using an unbiased mass spectrometry secretome analysis of cancer educated macrophages, we identified the glycoprotein granulin. Granulin has previously been associated with fibroblast activation and migration during wound healing 40. In addition, in breast cancer, granulin expression correlates with increased fibrosis and poor survival 5, 41. In agreement with a role for granulin in fibrosis, we found that macrophage secreted granulin plays a critical role in PDAC metastasis by activating resident hStCs and stimulating the secretion of periostin. The precise signalling pathway by which granulin activates hStCs and primary fibroblasts remains unknown, as the cognate cell-surface receptor to which granulin binds is still controversial 49–51. Interestingly, depletion of granulin in the hematopoietic compartment did not change macrophage recruitment to the liver, macrophage polarisation, or CD8+ T cell infiltration (Fig. 5 and Supplementary Fig. 7).

In agreement with Costa-Silva et al 52, we found that macrophages play a key role in PDAC metastasis. While Costa-Silva and colleagues 52 describe a role for resident hepatic macrophages in the establishment of a pre-metastatic niche that facilitates initial tumour cells seeding, our work focuses on understanding the subsequent step of metastatic growth. In this respect, we found that once tumour cells have reached the metastatic site, their survival and outgrowth capacity critically depends on the further recruitment of IM that secrete granulin.

Unfortunately, current imaging approaches are unable to detect micro-metastases and by the time pancreatic cancer patients are diagnosed, micro-metastatic spreading has already occurred in the majority of cases 1. Our findings suggest that recruitment of IM that express granulin plays a key role in pancreatic cancer metastasis and may serve both as a prognostic marker, and a potential target for PDAC liver metastasis.

Supplementary Material

Refer to Web version on PubMed Central for supplementary material.

Acknowledgements

We thank the flow cytometry and cell sorting facility and the animal facility at the University of Liverpool for provision of equipment and technical assistance. We are grateful to Jin Young Kim and Jong Shin Yoo at the Korea Basic Science Institute, Mass Spectrometry Research Centre, for their assistance. We acknowledge the Liverpool

Tissue Bank for provision of tissue samples. We thank A. Taylor and P. Murray, University of Liverpool, for technical help with lentiviral particle infection. We thank Lisa Young, CRUK Cambridge Research Institute, for assistance with animal models. We also thank the patients and their families, as well as the healthy blood donors who contributed with tissue samples and blood donations to these studies. These studies were supported by grants from the Medical Research Council (grant number MR/L000512/1) and the Pancreatic Cancer Research Fund (M.C.S.), the National Institute for Health Research Biomedical Research Unit funding scheme through a NIHR Pancreas BRU/Cancer Research UK PhD fellowship (S.R.N.), North West Cancer Research (M.C.S. and V.Q.), and a Sir Henry Dale Fellowship jointly funded by the Wellcome Trust and the Royal Society (A.M., grant number 102521/Z/13/Z).

References

1. Ryan DP, Hong TS, Bardeesy N. Pancreatic adenocarcinoma. The New England journal of medicine. 2014; 371:2140–2141. [PubMed: 25427123]
2. Von Hoff DD, et al. Increased survival in pancreatic cancer with nab-paclitaxel plus gemcitabine. The New England journal of medicine. 2013; 369:1691–1703. [PubMed: 24131140]
3. Vanharanta S, Massague J. Origins of metastatic traits. Cancer cell. 2013; 24:410–421. [PubMed: 24135279]
4. Nguyen DX, Bos PD, Massague J. Metastasis: from dissemination to organ-specific colonization. Nature reviews. Cancer. 2009; 9:274–284. [PubMed: 19308067]
5. McAllister SS, Weinberg RA. The tumour-induced systemic environment as a critical regulator of cancer progression and metastasis. Nat Cell Biol. 2014; 16:717–727. [PubMed: 25082194]
6. Quail DF, Joyce JA. Microenvironmental regulation of tumor progression and metastasis. Nat Med. 2013; 19:1423–1437. [PubMed: 24202395]
7. Erler JT, et al. Hypoxia-induced lysyl oxidase is a critical mediator of bone marrow cell recruitment to form the premetastatic niche. Cancer cell. 2009; 15:35–44. [PubMed: 19111879]
8. Malanchi I, et al. Interactions between cancer stem cells and their niche govern metastatic colonization. Nature. 2012; 481:85–89. [PubMed: 22158103]
9. Kitamura T, Qian BZ, Pollard JW. Immune cell promotion of metastasis. Nature reviews. Immunology. 2015; 15:73–86.
10. Sevenich L, et al. Analysis of tumour- and stroma-supplied proteolytic networks reveals a brain-metastasis-promoting role for cathepsin S. Nat Cell Biol. 2014; 16:876–888. [PubMed: 25086747]
11. Qian BZ, et al. CCL2 recruits inflammatory monocytes to facilitate breast-tumour metastasis. Nature. 2011; 475:222–225. [PubMed: 21654748]
12. Qian BZ, Pollard JW. Macrophage diversity enhances tumor progression and metastasis. Cell. 2010; 141:39–51. [PubMed: 20371344]
13. Kitamura T, et al. CCL2-induced chemokine cascade promotes breast cancer metastasis by enhancing retention of metastasis-associated macrophages. The Journal of experimental medicine. 2015; 212:1043–1059. [PubMed: 26056232]
14. Kim S, et al. Carcinoma-produced factors activate myeloid cells through TLR2 to stimulate metastasis. Nature. 2009; 457:102–106. [PubMed: 19122641]
15. Ohlund D, Elyada E, Tuveson D. Fibroblast heterogeneity in the cancer wound. The Journal of experimental medicine. 2014; 211:1503–1523. [PubMed: 25071162]
16. Pellicoro A, Ramachandran P, Iredale JP, Fallowfield JA. Liver fibrosis and repair: immune regulation of wound healing in a solid organ. Nature reviews. Immunology. 2014; 14:181–194.
17. Olive KP, et al. Inhibition of Hedgehog signaling enhances delivery of chemotherapy in a mouse model of pancreatic cancer. Science. 2009; 324:1457–1461. [PubMed: 19460966]
18. Sherman MH, et al. Vitamin d receptor-mediated stromal reprogramming suppresses pancreatitis and enhances pancreatic cancer therapy. Cell. 2014; 159:80–93. [PubMed: 25259922]
19. Erez N, Truitt M, Olson P, Arron ST, Hanahan D. Cancer-Associated Fibroblasts Are Activated in Incipient Neoplasia to Orchestrate Tumor-Promoting Inflammation in an NF-kappaB-Dependent Manner. Cancer cell. 2010; 17:135–147. [PubMed: 20138012]
20. Ozdemir BC, et al. Depletion of carcinoma-associated fibroblasts and fibrosis induces immunosuppression and accelerates pancreas cancer with reduced survival. Cancer Cell. 2014; 25:719–734. [PubMed: 24856586]

21. Rhim AD, et al. Stromal elements act to restrain, rather than support, pancreatic ductal adenocarcinoma. Cancer cell. 2014; 25:735–747. [PubMed: 24856585]
22. Neoptolemos JP. A randomized trial of chemoradiotherapy and chemotherapy after resection of pancreatic cancer (vol 350, pg 1200, 2004). New Engl J Med. 2004; 351:726–726.
23. Sperti C, Pasquali C, Piccoli A, Pedrazzoli S. Recurrence after resection for ductal adenocarcinoma of the pancreas. World J Surg. 1997; 21:195–200. [PubMed: 8995078]
24. Hingorani SR, et al. Trp53R172H and KrasG12D cooperate to promote chromosomal instability and widely metastatic pancreatic ductal adenocarcinoma in mice. Cancer cell. 2005; 7:469–483. [PubMed: 15894267]
25. Lim C, et al. Tumour progression and liver regeneration--insights from animal models. Nature reviews. Gastroenterology & hepatology. 2013; 10:452–462. [PubMed: 23567217]
26. Little EC, et al. Novel immunocompetent murine models representing advanced local and metastatic pancreatic cancer. J Surg Res. 2012; 176:359–366. [PubMed: 22221605]
27. Geissmann F, et al. Development of monocytes, macrophages, and dendritic cells. Science. 2010; 327:656–661. [PubMed: 20133564]
28. Hashimoto D, et al. Tissue-resident macrophages self-maintain locally throughout adult life with minimal contribution from circulating monocytes. Immunity. 2013; 38:792–804. [PubMed: 23601688]
29. Yona S, et al. Fate mapping reveals origins and dynamics of monocytes and tissue macrophages under homeostasis. Immunity. 2013; 38:79–91. [PubMed: 23273845]
30. Schulz C, et al. A lineage of myeloid cells independent of Myb and hematopoietic stem cells. Science. 2012; 336:86–90. [PubMed: 22442384]
31. Klein I, et al. Kupffer cell heterogeneity: functional properties of bone marrow derived and sessile hepatic macrophages. Blood. 2007; 110:4077–4085. [PubMed: 17690256]
32. Corbett TH, et al. Induction and chemotherapeutic response of two transplantable ductal adenocarcinomas of the pancreas in C57BL/6 mice. Cancer research. 1984; 44:717–726. [PubMed: 6692374]
33. Hirsch E, et al. Central role for G protein-coupled phosphoinositide 3-kinase gamma in inflammation. Science. 2000; 287:1049–1053. [PubMed: 10669418]
34. Camps M, et al. Blockade of PI3Kgamma suppresses joint inflammation and damage in mouse models of rheumatoid arthritis. Nat Med. 2005; 11:936–943. [PubMed: 16127437]
35. Schmid MC, et al. Receptor tyrosine kinases and TLR/IL1Rs unexpectedly activate myeloid cell PI3kgamma, a single convergent point promoting tumor inflammation and progression. Cancer cell. 2011; 19:715–727. [PubMed: 21665146]
36. van Rooijen N, van Nieuwmegen R. Elimination of phagocytic cells in the spleen after intravenous injection of liposome-encapsulated dichloromethylene diphosphonate. An enzyme-histochemical study. Cell Tissue Res. 1984; 238:355–358. [PubMed: 6239690]
37. Shree T, et al. Macrophages and cathepsin proteases blunt chemotherapeutic response in breast cancer. Genes & development. 2011; 25:2465–2479. [PubMed: 22156207]
38. Coussens LM, Tinkle CL, Hanahan D, Werb Z. MMP-9 supplied by bone marrow-derived cells contributes to skin carcinogenesis. Cell. 2000; 103:481–490. [PubMed: 11081634]
39. Hildenbrand R, Wolf G, Bohme B, Bleyl U, Steinborn A. Urokinase plasminogen activator receptor (CD87) expression of tumor-associated macrophages in ductal carcinoma in situ, breast cancer, and resident macrophages of normal breast tissue. J Leukoc Biol. 1999; 66:40–49. [PubMed: 10410988]
40. He Z, Ong CH, Halper J, Bateman A. Progranulin is a mediator of the wound response. Nat Med. 2003; 9:225–229. [PubMed: 12524533]
41. Elkabets M, et al. Human tumors instigate granulin-expressing hematopoietic cells that promote malignancy by activating stromal fibroblasts in mice. The Journal of clinical investigation. 2011; 121:784–799. [PubMed: 21266779]
42. Hellerbrand C, Stefanovic B, Giordano F, Burchardt ER, Brenner DA. The role of TGFbeta1 in initiating hepatic stellate cell activation in vivo. J Hepatol. 1999; 30:77–87. [PubMed: 9927153]

43. Gidekel Friedlander SY, et al. Context-dependent transformation of adult pancreatic cells by oncogenic K-Ras. Cancer cell. 2009; 16:379–389. [PubMed: 19878870]
44. Bao S, et al. Periostin potently promotes metastatic growth of colon cancer by augmenting cell survival via the Akt/PKB pathway. Cancer cell. 2004; 5:329–339. [PubMed: 15093540]
45. Gordon S, Taylor PR. Monocyte and macrophage heterogeneity. Nature reviews. Immunology. 2005; 5:953–964.
46. DeNardo DG, et al. Leukocyte complexity predicts breast cancer survival and functionally regulates response to chemotherapy. Cancer discovery. 2011; 1:54–67. [PubMed: 22039576]
47. Pyonteck SM, et al. CSF-1R inhibition alters macrophage polarization and blocks glioma progression. Nat Med. 2013; 19:1264–1272. [PubMed: 24056773]
48. Schmid MC, et al. Combined blockade of integrin-alpha4beta1 plus cytokines SDF-1alpha or IL-1beta potently inhibits tumor inflammation and growth. Cancer research. 2011; 71:6965–6975. [PubMed: 21948958]
49. Etemadi N, Webb A, Bankovacki A, Silke J, Nachbur U. Progranulin does not inhibit TNF and lymphotoxin-alpha signalling through TNF receptor 1. Immunology and cell biology. 2013; 91:661–664. [PubMed: 24100384]
50. Tang W, et al. The growth factor progranulin binds to TNF receptors and is therapeutic against inflammatory arthritis in mice. Science. 2011; 332:478–484. [PubMed: 21393509]
51. Chen X, et al. Progranulin does not bind tumor necrosis factor (TNF) receptors and is not a direct regulator of TNF-dependent signaling or bioactivity in immune or neuronal cells. J Neurosci. 2013; 33:9202–9213. [PubMed: 23699531]
52. Costa-Silva B, et al. Pancreatic cancer exosomes initiate pre-metastatic niche formation in the liver. Nat Cell Biol. 2015; 17:816–826. [PubMed: 25985394]

Europe PMC Funders Author Manuscripts

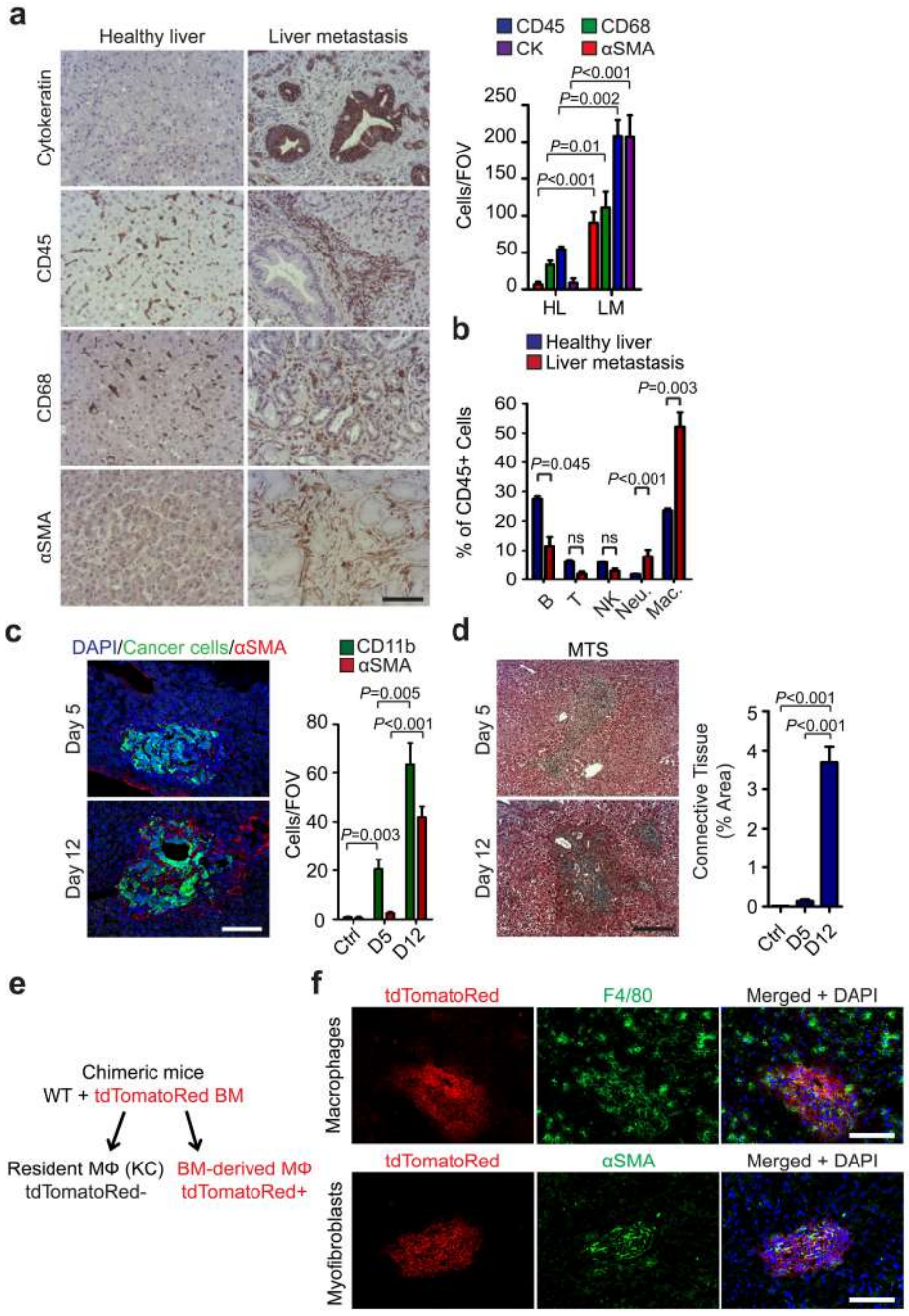

Figure 1. Metastatic PDAC cells induce macrophage recruitment and activation of myofibroblasts in the liver

(a) Identification of pan-cytokeratin $(CK)^+$ metastatic pancreatic cancer cells, hematopoietic cells ($CD45^+$), macrophages ($CD68^+$) and myofibroblasts (αSMA^+) as predominant cell types at the hepatic metastatic microenvironment of pancreatic cancer by immunohistochemical analysis of human biopsies. Representative micrographs and quantification of the data are shown (n = 5 PDAC patients, n= 5 healthy subjects; five fields assessed per sample; mean ± s.e.m; two-tailed unpaired t-test). HL= healthy liver, LM= liver metastasis.

(b) Established metastatic nodules in the liver were processed 12 days post intrasplenic implantation of $1x10^6$ KPC and analysed by flow cytometry. Composition of intrametastatic leukocytes is shown as a percentage of CD45+ cells using the following definitions: B cells ($CD45^+CD3^{neg}B220^+$); T cells ($CD45^+B220^{neg}CD3^+$), NK cells ($CD45^+B220^{neg}CD3^{neg}NK1.1^+$), Neutrophils ($CD11b^+Ly6G^+F4/80^{neg}$), MAMs ($CD11b^+F4/80^+$) (n= 4 healthy livers; n = 8 liver metastasis; data combine two independent experiments; mean ± s.e.m; two-tailed unpaired t-test).

(c) Representative immunofluorescence staining of myofibroblasts (αSMA^+) clustering around metastatic $KPC^{luc/zsGreen}$ (zsGreen) cells in the liver at 5 and 12 days after implantation. Histogram: quantification of myeloid cells ($CD11b^+$) and myofibroblasts (αSMA^+) cell frequency in livers during the course of metastasis formation. Nuclei were counterstained with DAPI (n = 6 mice per time point; four fields assessed per sample; data combine two independent experiments; mean ± s.e.m; two-tailed unpaired t-test).

(d) Representative Masson's trichrome staining of tumour bearing livers at 5 and 12 days after implantation. Histogram: quantification of area occupied by fibrotic stroma (n = 6 mice per time point; four fields assessed per sample; data combine two independent experiments; mean ± s.e.m; two-tailed unpaired t-test).

(e) Schematic of the generation of chimeric mice resulting in tdTomatoRed positive BM derived macrophages and non-labelled resident Kupffer cells (KC).

(f) Chimeric mice from (e) were intrasplenically implanted with $1x10^6$ Panc02 cells and livers were harvested after day 12. Immunofluorescence analysis of bone marrow derived $tdTomatoRed^+$ cells in combination with F4/80 staining and αSMA staining in tumour bearing livers. Nuclei were counterstained with DAPI (data are from 6 mice per condition; one experiment).

Scale bars = 100μm; ns, not significant.

Europe PMC Funders Author Manuscripts

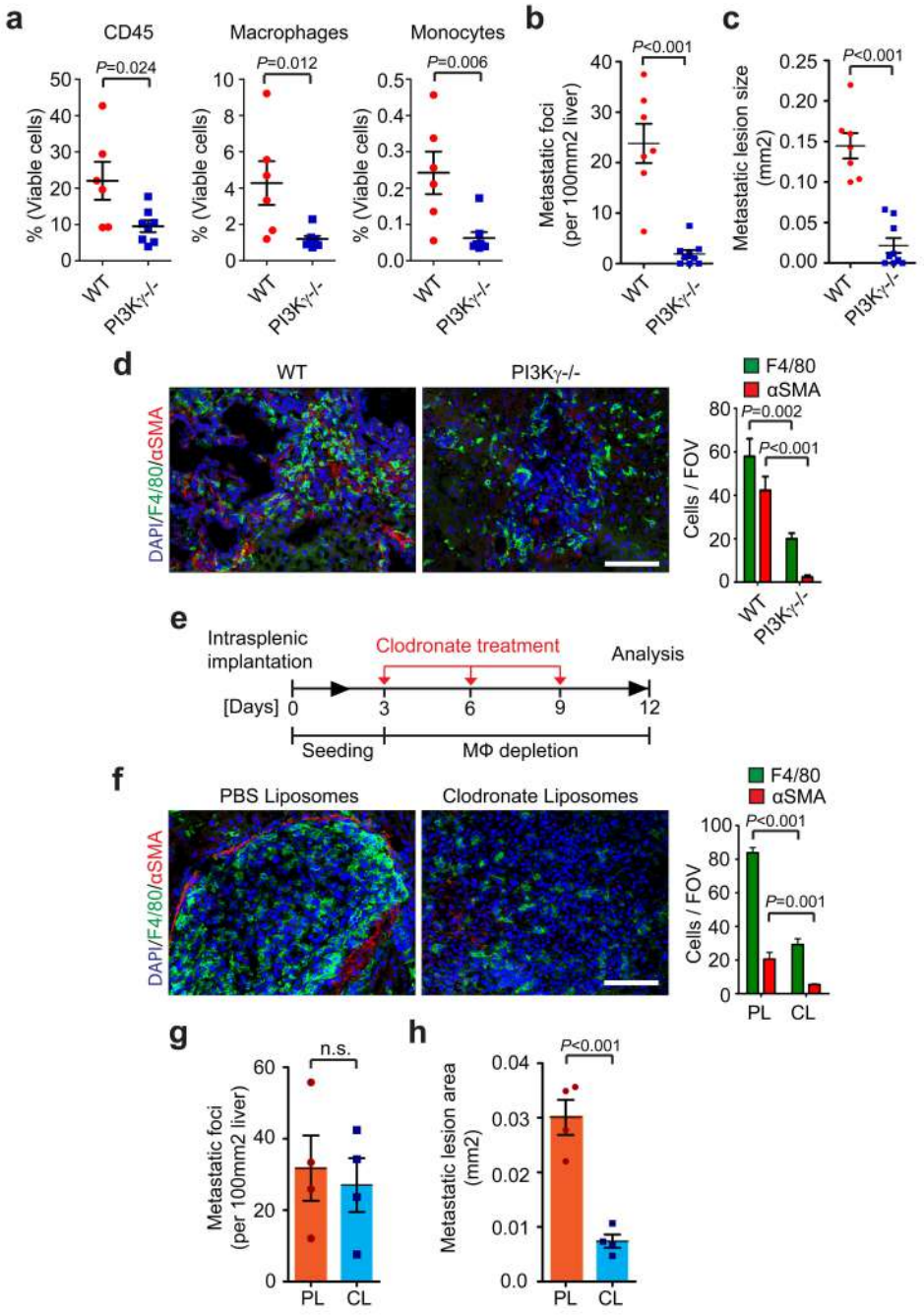

Figure 2. Macrophages promote myofibroblast activation and metastatic growth

(a - d) Liver metastasis was induced by intrasplenic implantation of $1x10^6$ KPC cells. Entire livers were harvested and analysed 12 days later.

(a) Hematopoietic cells ($CD45^+$), MAMs ($CD45^+CD11b^+F4/80^+$), and IM ($CD45^+CD11b^+Ly6C^+F4/80^{neg}Ly6G^{neg}$) from tumour bearing livers of wild type (WT) versus PI3K$\gamma^{-/-}$ (-/-) mice were evaluated by flow cytometry (n = 6 mice WT; n = 8 mice PI3K$\gamma^{-/-}$; data combine two independent experiments; individual data points, horizontal lines represent mean ± s.e.m; two-tailed unpaired t-test).

(b, c) Quantification of metastatic frequency (b) and average metastatic lesion size (c) in WT and PI3K$\gamma^{-/-}$ (-/-) mice by HE stained liver sections (n = 7 mice WT; n = 9 mice PI3K$\gamma^{-/-}$; data combine two independent experiments; mean ± s.e.m; two-tailed unpaired t-test).
(d) Representative immunofluorescence staining and quantification of MAMs (F4/80^{+}) and myofibroblasts (αSMA^{+}) cell frequency in livers in WT and PI3K$\gamma^{-/-}$ (-/-). Nuclei were counterstained with DAPI (n = 6 mice WT; n = 8 mice PI3K$\gamma^{-/-}$; four fields assessed per sample; data combine two independent experiments; mean ± s.e.m; two-tailed unpaired t-test).
(e - h) Liver metastasis was induced by intrasplenic implantation of 1x10^{6} KPC cells. Macrophages were depleted by clodronate liposome treatment after initial colonization of the liver had occurred.
(e) Schematic illustration of the experiment.
(f) Representative immunofluorescent staining and quantification of MAMs (F4/80^{+}) and myofibroblasts (αSMA^{+}) cell frequency in tumour bearing livers treated with liposomes containing PBS (PL) or clodronate (CL). Nuclei were counterstained with DAPI (n = 4 mice per condition; five fields assessed per sample; one experiment; mean ± s.e.m; two tailed unpaired t-test).
(g, h) Evaluation of metastatic frequency (g) and area covered by metastatic cells (h) in tumour bearing livers of mice treated with PL or CL (n = 4 mice per condition; all metastatic nodules assessed from one section per sample; one experiment; individual data and mean ± s.e.m; two-tailed unpaired t-test).
Scale bars = 100μm; ns, not significant.

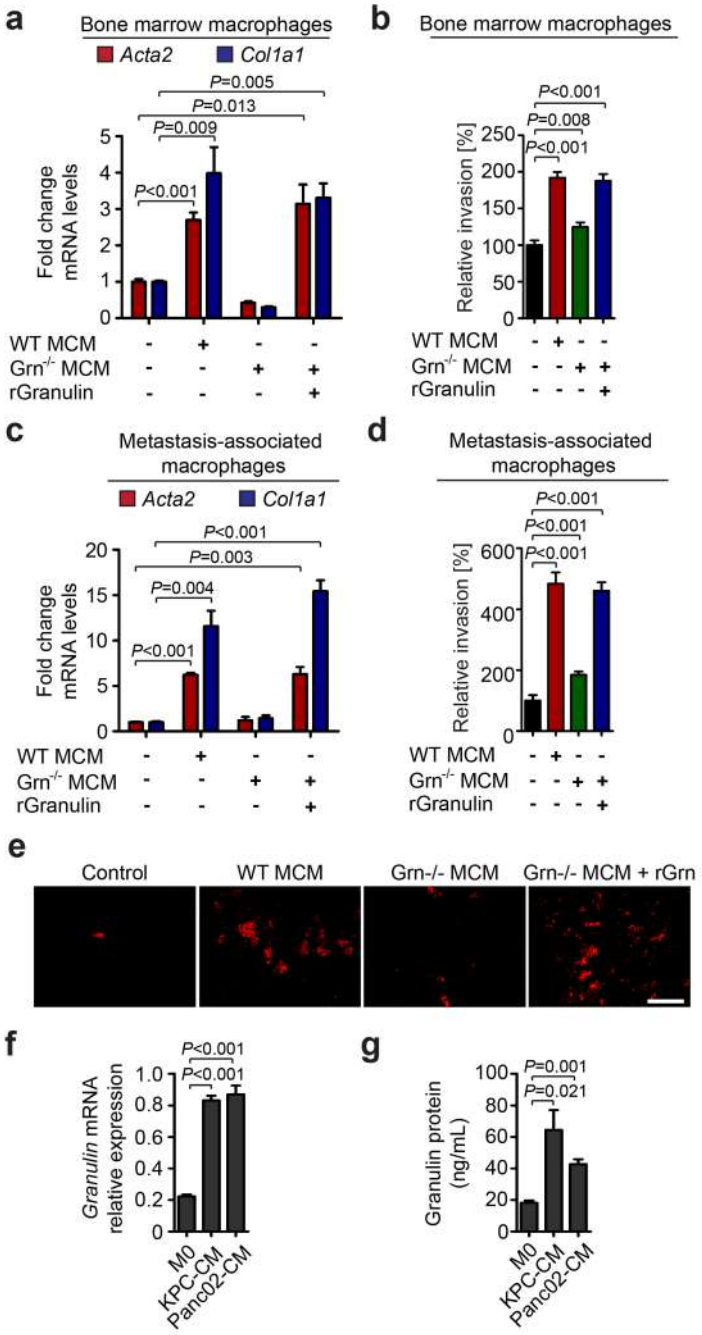

Figure 3. Granulin secreted by macrophages activates hepatic stellate cells

(a) Quantification of αSMA (*Acta2*), and collagen 1a (*Col1a*) mRNA levels in primary hStCs stimulated with isogenic macrophage conditioned media (MCM) generated from wild type (WT) or granulin deficient ($Grn^{-/-}$) macrophages, and CM generated from $Grn^{-/-}$ macrophages in the presence of recombinant granulin (rGranulin) as determined by qPCR (n = 3 independent experiments; mean ± s.e.m.; two-tailed unpaired t-test).

Europe PMC Funders Author Manuscripts

(b) Quantification hStCs invasion towards MCM generated from WT or $Grn^{-/-}$ deficient macrophages and MCM generated from $Grn^{-/-}$ in the presence of rGranulin (n = 3 independent experiments; mean ± s.e.m.; two-tailed unpaired t-test).
(c, d) same as (a, b), but MCM was generated using *in vivo* derived MAMs. Therefore liver metastasis was induced by intrasplenic implantation of $1x10^6$ KPC cells into isogenic WT + WT BM and WT + $Grn^{-/-}$ BM chimeric mice (n = 3 independent experiments; mean ± s.e.m.; two-tailed unpaired t-test).
(e) Representative immunofluorescence images of (d) showing Vybrant Dil (Em565) labelled murine hStCs showing invasion towards MCM generated from WT and Grn-/- MAMs and MCM generated from Grn-/- MAMs in the presence of recombinant granulin (rGranulin) (data are from three independent experiments).
(f, g) Quantification of *granulin* mRNA levels by qPCR (f) and granulin secretion by ELISA (g) in primary unstimulated (M0) macrophages and macrophages stimulated with isogenic CM media generated from murine KPC and Panc02 tumour cells (n = 3 independent experiments; mean ± s.e.m.; two-tailed unpaired t-test).
Scale bar = 100 μm; ns, not significant.

Europe PMC Funders Author Manuscripts

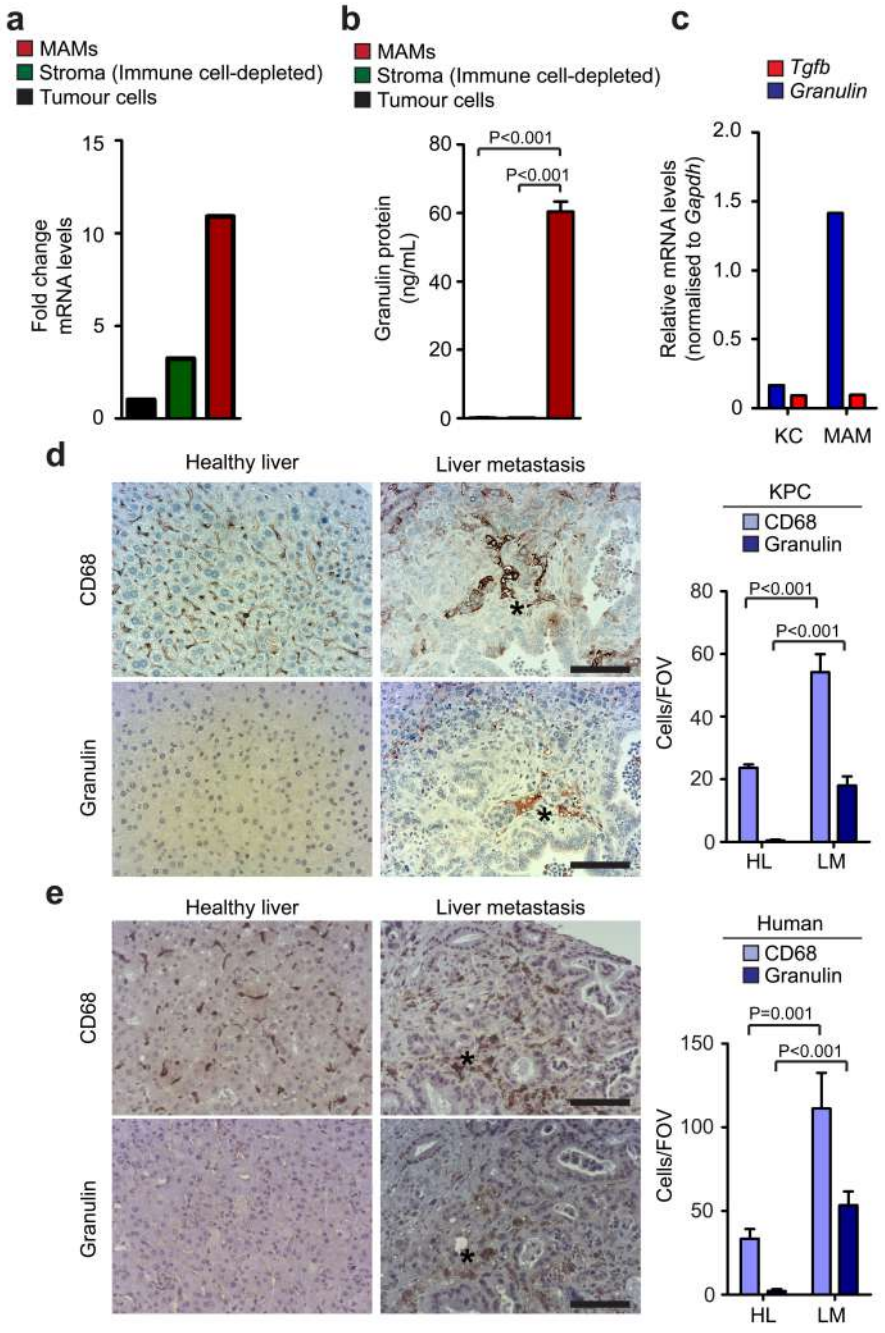

Figure 4. Granulin is highly expressed in hepatic metastatic lesions and metastasis associated macrophages are the main source of granulin secretion

(a, b) Quantification of *granulin* mRNA levels (a) and granulin protein levels (b) in intrametastatic pancreatic cancer cells, immune cell depleted stromal cells ($zsGreen^{neg}CD45^{neg}$), and MAMs ($CD45^{+}F4/80^{+}$) isolated by fluorescence activated cell sorting from established tumour bearing livers 12 days after intrasplenic implantation of $1x10^{6}$ $KPC^{luc/zsGreen}$ cancer cells (a, data are from three pooled mice; one experiment; b, n = 3 independent experiments; mean ± s.e.m.; two-tailed unpaired t-test).

Europe PMC Funders Author Manuscripts

(c) Quantification of *granulin* and *Tgfb* mRNA levels in tissue resident (KC) and MAMs sorted from established metastatic lesions from chimeric WT mice harbouring tdTomatoRed + BM as described in Fig. 1g (data are from three pooled mice; one experiment).
(d) Spontaneous metastatic hepatic tumours derived from KPC mice were isolated and analysed. Representative images of immunohistochemistry staining for MAMs ($CD68^+$) and granulin expression on serial tissue sections from metastatic lesions and healthy liver and quantification of the data (n = 5 control mice, n = 5 KPC mice, five fields assessed per sample; mean ± s.e.m.; two-tailed unpaired t-test).
(e) Representative images of immunohistochemistry staining for MAMs ($CD68^+$) and granulin expression on serial tissue sections from human metastatic PDAC lesions and healthy liver and quantification of the data (n = 5 healthy subjects, n = 5 PDAC samples; five fields assessed per sample; mean ± s.e.m.; two-tailed unpaired t-test).
Scale bars = 100μm; asterisks indicate matched tissue areas; ns, not significant.

Europe PMC Funders Author Manuscripts

Europe PMC Funders Author Manuscripts

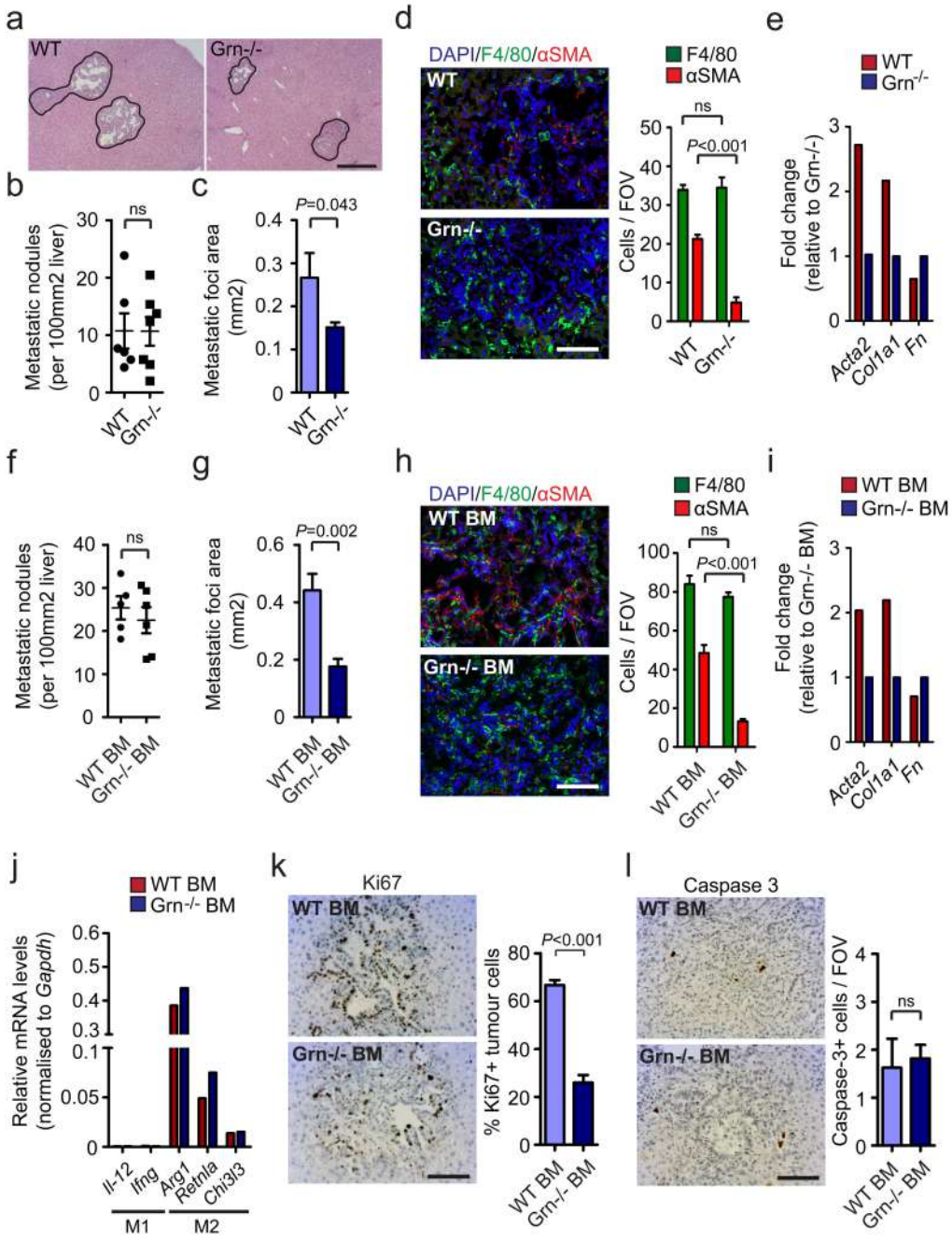

Figure 5. Granulin depletion prevents myofibroblast activation and PDAC metastasis

Liver metastasis was induced by intrasplenic implantation of $5x10^5$ KPC cells into WT and granulin deficient ($Grn^{-/-}$;) mice (a – e) and chimeric WT + WT BM and WT + $Grn^{-/-}$ BM mice (f – l). Entire livers were harvested and analysed 12 days later.

(a) Representative images of HE staining of liver sections (data are from 6 WT and 7 Grn-/- mice; one experiment).

(b) Metastatic frequency (n = 6 WT mice, n = 7 $Grn^{-/-}$ mice; all metastatic nodules assessed from one section per sample; one experiment; individual data points, horizontal lines represent mean ± s.e.m; two-tailed unpaired t-test).
(c) Metastatic area (n = 6 WT mice, n = 7 $Grn^{-/-}$ mice; all metastatic nodules assessed from one section per sample; one experiment; mean ± s.e.m; two-tailed unpaired t-test).
(d) Representative immunofluorescent staining and quantification of MAMs ($F4/80^{+}$) and myofibroblasts (αSMA^{+}) cell frequency in tumour bearing livers. Nuclei were counterstained with DAPI (n = 6 WT mice, n = 7 $Grn^{-/-}$ mice; four fields assess per sample; one experiment; mean ± s.e.m; two-tailed unpaired t-test).
(e) qPCR analysis of multiple hStCs activation markers in intrametastatic myofibroblasts isolated from established metastatic lesions (data are from three pooled mice per condition; one experiment).
(f) Metastatic frequency (n = 5 WT + WT BM mice, n = 6 WT + $Grn^{-/-}$ BM mice; all metastatic nodules assessed from one section per sample; one experiment; individual data points, horizontal lines represent mean ± s.e.m; two-tailed unpaired t-test).
(g) Metastatic area (n = 5 WT + WT BM mice, n = 6 WT + $Grn^{-/-}$ BM mice; all metastatic nodules assessed from one section per sample; one experiment; mean ± s.e.m; two-tailed unpaired t-test).
(h) Representative immunofluorescence staining and quantification of MAMs ($F4/80^{+}$) and myofibroblasts (αSMA^{+}) cell frequency in tumour bearing livers. Nuclei were counterstained with DAPI (n = 5 WT + WT BM mice, n = 6 WT + $Grn^{-/-}$ BM mice; four fields assessed per sample; one experiment; mean ± s.e.m; two-tailed unpaired t-test).
(i) qPCR analysis of multiple hStCs activation markers in intrametastatic myofibroblasts isolated from established metastatic lesions (data are from five pooled mice per condition; one experiment).
(j, k) Representative IHC staining and quantification of Ki67+ tumour cell frequency (j) and cleaved caspase 3+ cell numbers (k) in metastatic livers (n = 5 WT + WT BM mice, n = 6 WT + $Grn^{-/-}$ BM mice; five fields assessed per sample; one experiment; mean ± s.e.m; two-tailed unpaired t-test).
(l) qPCR analysis of multiple M2- and M1- macrophage associated genes in MAMs isolated from metastatic tumours developed in WT + WT BM and WT + $Grn^{-/-}$ BM mice (data are from 6 pooled mice per condition; one experiment).
Scale bars = 100μm; ns, not significant.

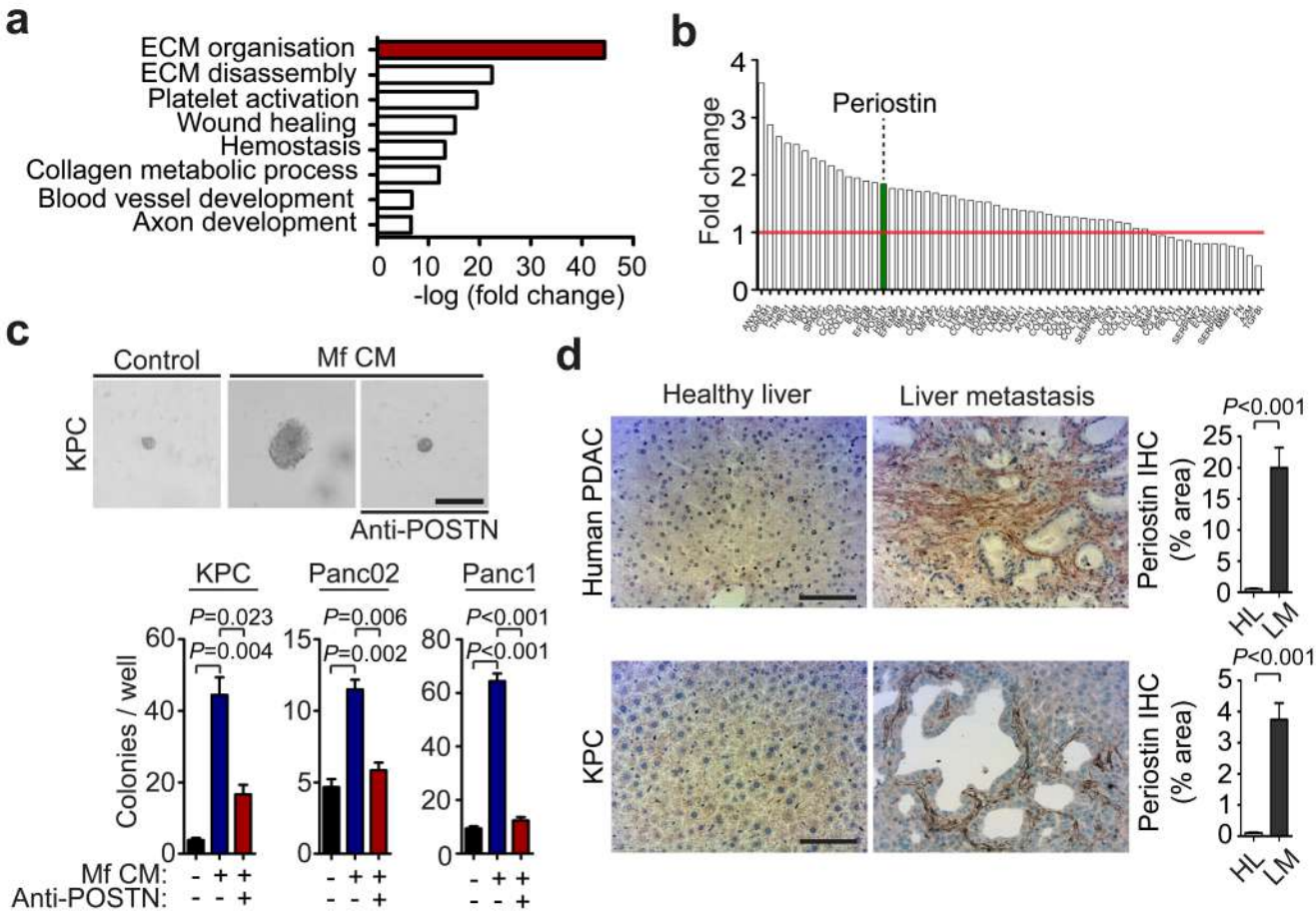

Figure 6. Myofibroblast secreted periostin enhances pancreatic cancer cell growth.

(a) Top gene ontology (GO) functions of secreted proteins enriched in human myofibroblasts (Mf) following *in vitro* education with macrophage conditioned media (CM).

(b) Fold change rank of identified proteins associated with extracellular matrix organisation. Data were obtained from one experiment assessing two biologically independent samples (Green = periostin).

(c) Colony formation assay of primary murine KPC cells, murine Panc02, and human Panc1 cells in the presence or absence of Mf CM and periostin neutralising antibody (anti-Periostin). Representative images reflecting colonies and single cells are displayed for KPC cells (n = 3 independent experiments; mean ± s.e.m; two-tailed unpaired t-test).

(d) Immunohistochemical stainings of periostin in human liver biopsies (n = 5 healthy subjects, n= 5 PDAC; five fields assessed per sample; mean ± s.e.m; two-tailed unpaired t-test) and in spontaneous metastatic liver tumours collected from KPC mice (n = 5 mice per condition; five fields assessed per sample, mean ± s.e.m; two-tailed unpaired t-test). Representative micrographs and quantification of the data. HL = healthy liver, LM = liver metastasis.

Scale bars = 100μm.

Europe PMC Funders Author Manuscripts

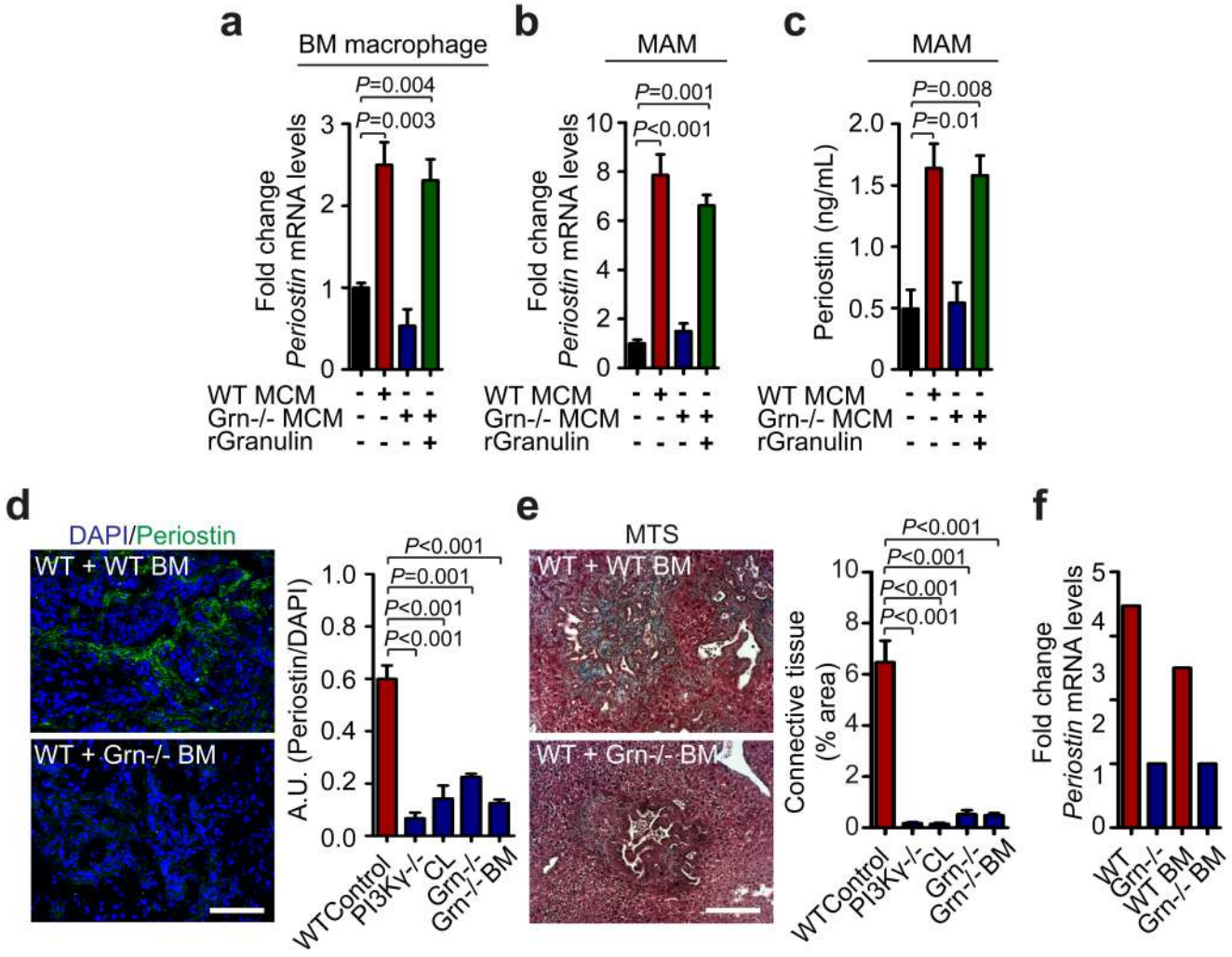

Figure 7. Macrophage derived granulin induces periostin expression by hepatic stellate cells *in vitro* and *in vivo*.

(a) Evaluation of periostin (*Postn*) mRNA expression levels in primary hStCs following stimulation with CM collected from BM WT or Grn$^{-/-}$ macrophages in the presence or absence of recombinant granulin (rGranulin) (n = 3 independent experiments; mean ± s.e.m.; two-tailed unpaired t-test).

(b, c) Evaluation of periostin (*Postn*) mRNA levels by qPCR (b) and periostin protein levels by ELISA (c) in primary hStCs following stimulation with CM collected from *in vivo* derived WT or Grn$^{-/-}$ MAMs, in the presence or absence of recombinant granulin (rGranulin) (n = 3 independent experiments; mean ± s.e.m.; two-tailed unpaired t-test).

(d, e) Evaluation of periostin deposition and fibrotic stroma formation in metastatic livers of control WT, WT mice treated with clodronate liposomes (CL), PI3K$\gamma^{-/-}$, Grn$^{-/-}$, and WT + Grn$^{-/-}$ BM mice 12 days after intrasplenic implantation of KPC cells. (d) Representative immunofluorescence staining and quantification of periostin deposition. Nuclei were counterstained with DAPI. (e) Representative Masson's trichrome staining (MTS) and quantification of area occupied by fibrotic stroma (n = 4 mice per condition; four fields

assessed per sample; data combine five independent experiments; mean ± s.e.m; two-tailed unpaired t-test).

(f) Quantification of periostin (*Postn*) mRNA expression levels by qPCR in intrametastatic myofibroblasts isolated from tumour bearing livers of WT and $Grn^{-/-}$ mice, and chimeric WT + WT BM and WT + $Grn^{-/-}$ BM mice (data are from six pooled mice per condition; one experiment).

Scale bars = 100μm.

Europe PMC Funders Author Manuscripts

Europe PMC Funders Author Manuscripts

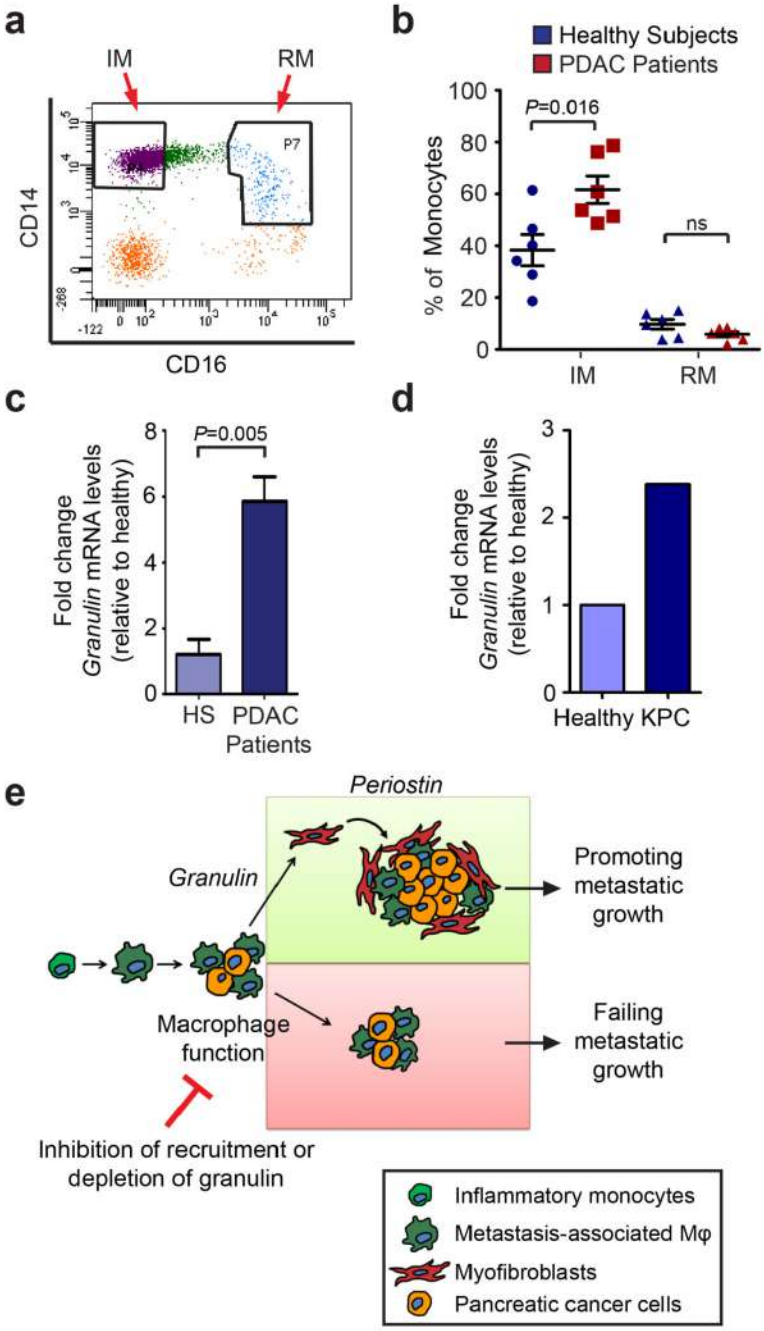

Figure 8. Metastatic PDAC patients have increased circulating inflammatory monocytes that express high levels of granulin

(a) Peripheral mononuclear cells were isolated from healthy subjects and metastatic PDAC patients. Representative dot plot of inflammatory monocytes (IM; $CD14^{hi}CD16^{neg}$) and resident monocytes (RM; $CD14^{dim}CD16^{hi}$) after gating for the $CD45^{+}CD3^{neg}B220^{neg}CD19^{neg}Sytox^{neg}$ cell population (data are from 6 different PDAC patients and 6 different healthy subjects).

(b) Quantification of a. Percentage of monocyte populations in healthy subjects and metastatic PDAC patients (n = 6 different healthy; n = 6 different PDAC samples; individual

data points, horizontal lines represent mean ± s.e.m.; two tailed unpaired t-test). NS, not significant.

(c) Quantification of *granulin* mRNA levels in inflammatory monocytes (IM) isolated from metastatic PDAC patients and healthy subjects (HS) as described in (a, b) (n = 3 different healthy, n = 4 different PDAC samples; mean ± s.e.m; two-tailed unpaired t-test).

(d) Quantification of *granulin* mRNA levels in circulating IM sorted from KPC mice with pathological confirmed liver metastasis or tumour free litter mates (data are from four pooled mice per condition; one experiment).

(e) Schematic depicting the role of macrophage-derived granulin in activation of hStCs and in PDAC liver metastasis. Inflammatory monocytes are recruited to the liver by metastatic pancreatic tumour cells through a PI3Kγ-dependent mechanism. Once in the metastatic tissue, differentiated macrophages stimulate the activation and recruitment of resident hStCs through granulin secretion resulting in excessive accumulation of myofibroblasts. Granulin-induced myofibroblasts release high levels of the extracellular matrix protein periostin, thereby enhancing survival and growth of metastatic pancreatic cancer cells in a hostile environment. Interruption of this sequence, by either preventing macrophage accumulation or by abolishing granulin expression in recruited macrophages, limits metastatic growth of pancreatic cancer cells.

Europe PMC Funders Author Manuscripts